HHS Public Access

Author manuscript

J Mol Cell Cardiol. Author manuscript; available in PMC 2018 February 01.

Published in final edited form as:

J Mol Cell Cardiol. 2017 February ; 103: 93–101. doi:10.1016/j.yjmcc.2017.01.006.

Early Remodeling of Repolarizing K+ Currents in the αMHC$^{403/+}$ Mouse Model of Familial Hypertrophic Cardiomyopathy

Rocco Hueneke[1,2], **Adam Adenwala**[1], **Rebecca L. Mellor**[1,3], **Jonathan G. Seidman**[4], **Christine E. Seidman**[4,5], and **Jeanne M. Nerbonne**[1,3,*]

[1]Department of Developmental Biology, Washington University Medical School, St. Louis, MO 63110-1093, USA

[2]Department of Anesthesiology, Washington University Medical School, St. Louis, MO 63110-1093, USA

[3]Department of Medicine, Washington University Medical School, St. Louis, MO 63110-1093, USA

[4]Department of Genetics, Harvard Medical School, 77 Avenue Louis Pasteur, Boston, MA 02115, USA

[5]Howard Hughes Medical Institute, Chevy Chase, MD 20815

Abstract

Familial hypertrophic cardiomyopathy (HCM), linked to mutations in myosin, myosin-binding proteins and other sarcolemmal proteins, is associated with increased risk of life threatening ventricular arrhythmias, and a number of animal models have been developed to facilitate analysis of disease progression and mechanisms. In the experiments here, we use the αMHC$^{403/+}$ mouse line in which one αMHC allele harbors a common HCM mutation (in βMHC, Arg403 Gln). Here, we demonstrate marked prolongation of QT intervals in young adult (10–12 week) male αMHC$^{403/+}$ mice, well in advance of the onset of measurable left ventricular hypertrophy. Electrophysiological recordings from myocytes isolated from the interventricular septum of these animals revealed significantly (P<0.001) lower peak repolarizing voltage-gated K^+ (Kv) current ($I_{K,peak}$) amplitudes, compared with cells isolated from wild type (WT) littermate controls. Analysis of Kv current waveforms revealed that the amplitudes of the inactivating components of the total outward Kv current, $I_{to,f}$, $I_{to,s}$ and $I_{K,slow}$, were significantly lower in αMHC$^{403/+}$, compared with WT, septum cells, whereas I_{ss} amplitudes were similar. The amplitudes/densities of $I_{K,peak}$ and $I_{K,slow}$ were also lower in αMHC$^{403/+}$, compared with WT, LV wall and LV apex myocytes, whereas $I_{to,f}$ was attenuated in αMHC$^{403/+}$ LV wall, but not LV apex, cells. These regional differences in the remodeling of repolarizing Kv currents in the αMHC$^{403/+}$ mice would

*Address correspondence to: Jeanne M. Nerbonne Departments of Medicine and Developmental Biology, Washington University Medical School, 660 South Euclid Avenue, Box 8086, St. Louis, MO 63110-1093, USA, Tel.: +1 314 362 2564, Fax: +1 314 362 0186, jnerbonne@wustl.edu.

Disclosures: No actual or potential conflicts of interest to disclose.

be expected to increase the dispersion of ventricular repolarization and be proarrhythmic. Quantitative RT-PCR analysis revealed reductions in the expression of transcripts encoding several K^+ channel subunits in the interventricular septum, LV free wall and LV apex of (10–12 week) $\alpha MHC^{403/+}$ mice, although this transcriptional remodeling was not correlated with the observed decreases in K^+ current amplitudes.

Keywords

Hypertrophy; Electrical remodeling; ECG; QT interval; Repolarization; Kv currents; Transcriptional remodeling

1. Introduction

Hypertrophic cardiomyopathy (HCM), the most common cause of sudden death in apparently healthy children and young adults [1], is characterized by left ventricular (LV) hypertrophy, which frequently involves the interventricular septum [2]. The histopathological features of HCM include cardiomyocyte hypertrophy, myofibril disarray, and interstitial fibrosis [3]. To date, more than 900 mutations in over 20 sarcomere related genes have been identified in familial HCM [3]. Among the causative genes, mutations in β-myosin heavy chain (βMHC) and myosin binding protein 3 (MYBP3) are the most common [4]. The clinical course of HCM patients is highly variable [2,3], ranging from individuals being asymptomatic well into adulthood to sudden cardiac death in adolescence, even in individuals harboring the same genetic mutation. Despite progress in preventing sudden death in high-risk HCM patients through the use of implantable cardioverter defibrillators (ICDs), it is unclear why mutations in genes encoding sarcomere proteins lead to the increased risk of life-threatening ventricular arrhythmias.

A number of animal models of familial HCM have been developed with the goal of facilitating the study of disease mechanisms [5]. The $\alpha MHC^{403/+}$ mouse line, for example, was engineered to carry the human MHC mutation Arg403Gln in one allele of the α-cardiac MHC gene, the murine analogue of human β-cardiac MHC gene [6]. Analysis of the cardiac phenotype in heterozygous $\alpha MHC^{403/+}$ mice revealed several features which closely parallel the human disease [6,7]. Specifically, LV hypertrophy is progressive, somewhat variable in presentation and, in addition, phenotypes are more pronounced in male, than in female, $\alpha MHC^{403/+}$ mice [8]. Myocyte enlargement, cardiac fibrosis and myofibril disarray have been reported to begin to be evident in male $\alpha MHC^{403/+}$ mice at about 15 weeks of age, and all male $\alpha MHC^{403/+}$ animals have echocardiographic evidence of LV hypertrophy by 25–30 weeks of age [9,10]. Previous electrocardiographic (ECG) studies revealed abnormalities in the ECG axis and prolongation of QT intervals in 30 week old $\alpha MHC^{403/+}$ mice [8,11]. In addition, ventricular tachyarrhythmias were induced by electrical pacing in about 70% of >30 week old male $\alpha MHC^{403/+}$ mice [9]. Ventricular tachyarrhythmias were also shown to be inducible in ~25% of the young (10 week old male) $\alpha MHC^{403/+}$ mice examined [9], i.e., at an age well before the onset of echocardiographically detectable LV hypertrophy, findings that suggest that electrical remodeling may be independent of LV hypertrophy in $\alpha MHC^{403/+}$ animals. Interestingly, several clinical studies have identified subsets of HCM

patients with marked QT prolongation, but without manifest LV hypertrophy, observations also consistent with the hypothesis that altered ventricular repolarization in HCM patients may also not be related solely to cardiac (ventricular myocyte) hypertrophy [12–15].

The experiments here were designed to explore the hypothesis that electrical remodeling precedes LV hypertrophy in the αMHC$^{403/+}$ mouse model of HCM. The results presented demonstrate that QT prolongation is present in young adult (10–12 week old) male αMHC$^{403/+}$ animals prior to measurable LV or ventricular myocyte hypertrophy. Additional experiments revealed that the amplitudes of the voltage-gated K^+ (Kv) currents that underlie action potential repolarization are significantly lower in interventricular septum, LV apex, and LV free wall myocytes isolated from 10–12 week old male αMHC$^{403/+}$, compared with WT, animals. Deleterious electrical remodeling, therefore, precedes and appears to be independent of the development of LV hypertrophy in this mouse model of HCM.

2. Methods

2.1. Experimental animals

Animals were handled in accordance with the Guide for the Care and Use of Laboratory Animals (NIH). All protocols involving animals were approved by the Animal Studies Committee at Washington University Medical School. The αMHC$^{403/+}$ mouse line, described previously [6], was maintained in the 129SvE background; for breeding, wildtype male and female 129SvE mice were obtained from Taconic (Germantown, NY). All experiments here were carried out on adult (10–12 week) male αMHC$^{403/+}$ and WT littermates.

2.2. 2-D Echocardiography

Anesthetized (avertin, 0.25 mg g^{-1}, intraperitoneal injection) (10–12 week old male) αMHC$^{403/+}$ (N = 8) and WT (N = 8) animals were examined by non-invasive transthoracic echocardiography using an Acuson Sequoia 256 echocardiography system (Acuson, Stockton, CA, USA) equipped with a 15 MHz transducer as described previously [16]. Digitally acquired and stored two-dimensional short axis cine-loops and M-mode images of the LV of αMHC$^{403/+}$ animals were viewed and displayed next to images obtained from age-matched WT littermates. Comparisons of LV wall thicknesses and chamber sizes in αMHC$^{403/+}$ and WT animals were completed.

2.3. Histology

For histological analyses, 10–12 week old male αMHC$^{403/+}$ (N = 2) and WT (N = 2) mice were anesthetized with intraperitoneal injection of ketamine (86 mg kg^{-1}) and xylazine (13 mg kg^{-1}) and perfused with 4% paraformaldehyde in 0.1 mol l^{-1} phosphate buffer. Isolated ventricular tissues were embedded in paraffin, sectioned (at 3 μM) and stained with Masson trichrome [16]. Ventricular myocyte cross-sectional areas were measured using an Axioskop upright (light) microscope (Carl Zeiss, Inc., Chester, VA, USA) and ImageJ software.

2.4. Electrophysiological recordings

Surface electrocardiographic (ECG) recordings were obtained from anesthetized (avertin, 0.25 mg kg-1, intraperitoneal injection) 10–12 week old male αMHC$^{403/+}$ (N = 15) and WT (N = 18) littermates using needle electrodes connected to a dual bioamplifier (PowerLab 26T, AD Instruments, Colorado Springs, CO, USA), as described previously [16]. ECG signals were acquired for 1 min; data were stored and subsequently analyzed offline using LabChart 7.1 (ADInstruments). Lead II recordings were chosen for analyses. In each record, QT intervals in individual beats were determined as the time interval between the initiation of the QRS complex and the end of the T wave, defined as the time the negative deflection of the T wave returned to the baseline [17,18]. Body weight, tibia length, and left ventricular (LV) weight were measured for each animal and recorded at the time of tissue harvesting.

Ventricular myocytes were isolated using previously described procedures [19,20]. Briefly, hearts were removed from anaesthetized (avertin, 0.25 mg kg-1, intraperitoneal injection) 10–12 week old male WT and αMHC$^{403/+}$ mice, mounted on a Langendorf apparatus and perfused retrogradely through the aorta with 25 ml of (0.8 mg ml^{-1}) collagenase-containing (type II, Worthington Biochemical Corp., Lakewood, NJ, USA) solution [19,20]. Following the perfusion, the LV free wall, LV apex and interventricular septum were separated using a fine scalpel and iridectomy scissors. Each of the tissue pieces was mechanically dispersed (separately), resuspended in Medium 199 (Sigma Chemical, St. Louis, MO, USA), plated on laminin-coated coverslips, and maintained in a 95%air-5%CO_2 incubator. Whole-cell voltage-clamp recordings were obtained from myocytes within 12 h of isolation at room temperature (22–24°C) [19,20]. All voltage-clamp experiments were performed using an Axopatch 1B amplifier (Molecular Devices, Sunnyvale, CA, USA), interfaced to a microcomputer with a Digidata 1332 analog/digital interface and the pCLAMP9 software package (Molecular Devices).

For recording of whole-cell K^+ currents, pipettes contained (in mM): KCl 135; EGTA 10; Hepes 10; K_2ATP 5; and glucose 5 (pH 7.2; 310 mosmol l^{-1}). The bath solution contained (in mM): NaCl 136; KCl 4; $MgCl_2$ 2; $CaCl_2$ 1; $CoCl_2$ 5; tetrodotoxin (TTX) 0.02; Hepes 10; and glucose 10 (pH 7.4; 300 mosmol l^{-1}). Whole-cell voltage-gated outward K^+ (Kv) currents, evoked in response to 4.5 s depolarizing voltage steps to test potentials between −60 and +40 mV (10 mV increments) from holding potential (HP) of −70 mV, were recorded, as previously described [19,20]. Depolarizing voltage steps were presented at 10 sec intervals to allow complete recovery of delayed rectifier Kv currents between sweeps [19,20]. Currents (I_{K1}) through inwardly rectifying K^+ (Kir) channels, evoked in response to hyperpolarization to −120 mV from the same HP, were also recorded from each cell [20]. Acquired voltage-clamp data were filtered a 5 kHz prior to digitization and storage, and subsequently analyzed offline using Clampfit (v. 9.2, Molecular Devices). Integration of the capacitive currents recorded during brief ± 10 mV voltage steps from −70 mV provided whole-cell membrane capacitances (C_m). Peak Kv current and I_{K1} amplitudes were measured as the maximal amplitudes of the outward and inward currents, respectively, evoked at each test potential under the recording conditions described above. The amplitudes of the Kv current components, $I_{to,f}$, $I_{to,s}$, $I_{K,slow}$, and I_{ss}, in individual interventricular septum, LV apex and LV wall myocytes (n values are provided in the Figure legends and in

Table 2), were determined from double or triple exponential fits to the decay phase of the outward K^+ currents, as previously described [19,20].. Current amplitudes were normalized to the whole-cell membrane capacitance (in the same cell) and current densities (in pA pF^{-1}) are also reported.

2.5. Transcript analyses

Total RNA from the interventricular septum, LV apex or LV free wall of (10–12 week) male αMHC$^{403/+}$ and WT mice was isolated and DNase treated using previously described methods [16]. RNA concentrations were determined by optical density measurements. Using equal amounts of RNA, transcript analysis of genes encoding K^+ channel pore-forming (α) and accessory subunits, markers of pathological hypertrophy, as well as of control genes, including glyceraldehyde 3-phosphate dehydrogenase (*Gapdh*) and hypoxanthine guanine phospho-ribosyl transferase (*Hprt*), was carried out using SYBR green RT-PCR in a two step process [16]. The primers used for the quantitative RT-PCR analyses are provided in Table 1. Transcript data were normalized to *Hprt* and analyzed using the threshold cycle (C_T) relative quantification method [16]. Results are expressed as mean ± SEM 2-ΔC_T (N = 6) values [16].

2.6. Statistical analyses

All electrophysiological, morphological, and transcript data are presented as mean ± SEM. Electrophysiological data from individual myocytes from different regions of the left ventricles from multiple animals were analyzed. The total numbers of cells (n) included in the analyses and the total numbers of animals (N) from which these cells were obtained are indicated in the Figure legends. In all experiments, the statistical significance of observed differences between experimental groups was evaluated using the Student's t test; a two-tailed P value <0.05 was considered statistically significant.

3. Results

3.1. LV hypertrophy is not evident in 10–12 week old male αMHC$^{403/+}$ mice

It has previously been reported that LV wall dimensions in 10–20 week old male αMHC$^{403/+}$ and age-matched wild-type (WT) mouse hearts are not significantly different [10]. These observations suggest that this age, in this mutant mouse line, corresponds to the pre-clinical phase of congenital hypertrophic cardiomyopathy, i.e., prior to evidence of cellular/ventricular hypertrophy [6,10]. To explore this hypothesis further and as background for the cellular electrophysiological ventricular studies, we examined the hearts of male αMHC$^{403/+}$ animals at 10–12 weeks in detail. Visual examination of echocardiographic images revealed no significant differences in the thickness of the posterior LV wall or the interventricular septum in 2D short axis cine loops of the LV of αMHC$^{403/+}$ and WT animals (Figure 1A). M-mode analysis of LV posterior wall thicknesses also revealed no differences, with mean ± SEM LV posterior wall thicknesses of 0.94 ± 0.04 mm (n = 5) and 0.89 ± 0.02 mm (n = 5) in αMHC$^{403/+}$ and WT mice, respectively (Figure 1B). The mean ± SEM left ventricular mass to tibia length ratios (LVM/TL) determined in 10–12 week old male αMHC$^{403/+}$ and WT animals were also similar (Figure 2C). In addition, histological measurements from trichrome-stained transverse sections of LV free wall and

interventricular septum (Figure 2A) revealed that mean ± SEM LV myocyte cross-sectional area is not significantly different in 10–12 week old male αMHC$^{403/+}$, compared with WT, hearts (Figure 2B). There is, therefore, no anatomical indication of LV hypertrophy in male αMHC$^{403/+}$ mice at 10–12 weeks of age (see **Discussion**).

3.2. QT interval prolongation in 10–12 week old αMHC$^{403/+}$ mice

To determine whether the systemic electrophysiological consequences of the expression of the mutant αMHC protein are already present in young (10–12 week) male αMHC$^{403/+}$ mice prior to any echocardiographic evidence of LV hypertrophy, surface electrocardiographic (ECG) recordings were obtained from anesthetized (10–12 week old) male αMHC$^{403/+}$ and WT animals. As illustrated in Figure 3, surface ECG recordings revealed that QT intervals are clearly prolonged in (10–12 week) αMHC$^{403/+}$ (Figure 3B), compared with WT (Figure 3A), mice. The mean ± SEM QT interval measured in αMHC$^{403/+}$ mice, for example, was 71 ± 2 ms (n = 15), significantly (P<0.001) longer than the value of 59 ± 1 ms measured in WT (n = 18) mice (Figure 3C). In contrast, there were no significant differences in mean ± SEM RR, PR, and/or QRS durations in (10–12 week) αMHC$^{403/+}$ and WT animals (Figure 3C).

3.3. Repolarizing K^+ current amplitudes are decreased in αMHC$^{403/+}$ LV myocytes

Whole-cell voltage-clamp recordings were obtained from myocytes isolated from the interventricular septum of 10–12 week old male αMHC$^{403/+}$ and WT mice; representative recordings are presented in Figure 4. As described in **Methods**, voltage-gated K^+ (Kv) currents were evoked in response to (4.5 sec) voltage steps to test potentials between −40 and +40 mV from a holding potential of −70 mV. Inwardly rectifying K^+ (Kir) currents (I_{K1}) evoked at −120 mV from the same holding potential were also recorded in each cell (Figure 4). The voltage-clamp protocol is illustrated below the current records in Figure 4, panels A and B.

As illustrated in the representative records presented in Figure 4, peak outward Kv ($I_{K,peak}$) current amplitudes at all test potentials were lower in the myocyte isolated from the interventricular septum of the αMHC$^{403/+}$ animal (Figure 4B), compared with the interventricular septum cell isolated from an age-matched WT mouse (Figure 4A). The mean ± SEM $I_{K,peak}$ amplitude was also significantly (P<0.001) lower in αMHC$^{403/+}$(n = 11), than in WT (n = 19), interventricular septum myocytes (Table 2). It has been shown previously that the decay phases of the Kv currents in mouse interventricular septum myocytes are best described by the sum of 3 exponentials, reflecting the inactivating currents $I_{to,f}$, $I_{to,s}$, and $I_{K,slow}$, and a noninactivating current, I_{ss} [19]. Kinetic analyses of the Kv currents in records such as those shown in Figure 4A and B revealed that mean ± SEM $I_{to,f}$, $I_{to,s}$ and $I_{K,slow}$ amplitudes were significantly lower in αMHC$^{403/+}$, compared with WT, interventricular septum myocytes (Figure 4C; Table 2). Mean ± SEM I_{ss} and I_{K1} amplitudes in αMHC$^{403/+}$ and WT interventricular septum myocytes, however, were not significantly different (Figure 4C; Table 2). Whole-cell membrane capacitance (C_m) values, determined from integration of the capacitive transients recorded during brief (25 ms) sub-threshold ± 10 mV voltage steps from −70 mV, were indistinguishable in αMHC$^{403/+}$ and WT interventricular septum myocytes, with mean ± SEM C_m values of 160 ± 7 pF (n = 11) and

148 ± 5 pF (n = 19), respectively (Table 2). Normalization of the amplitudes of the individual Kv and Kir current components to the measured C_m values (in the same cell) revealed that mean ± SEM $I_{K,peak}$, $I_{to,f}$, $I_{to,s}$, and $I_{K,slow}$ densities were significantly lower in αMHC$^{403/+}$, than in WT, interventricular septum myocytes (Figure 4F; Table 2). Mean ± SEM I_{ss} and I_{K1} densities in αMHC$^{403/+}$ and WT interventricular septum myocytes, in contrast, were not significantly different (Figure 4F; Table 2).

Additional experiments were completed to determine whether there were also effects on repolarizing K^+ current amplitudes in other regions of the LV of αMHC$^{403/+}$ animals. Using established protocols [19,20], identical to those described above, whole-cell voltage-clamp recordings were obtained from myocytes isolated from the LV free wall and the LV apex of young male αMHC$^{403/+}$ and age-matched WT (littermates) mice (Figure 5). Similar to the findings for interventricular septum myocytes, the mean ± SEM C_m values in αMHC$^{403/+}$ and WT LV free wall myocytes, as well as in αMHC$^{403/+}$ and WT LV apex myocytes, were not significantly different (Table 2). The mean ± SEM $I_{K,peak}$ amplitudes (and densities), however, were significantly lower in αMHC$^{403/+}$, compared to WT, LV free wall ($P< 0.01$) and apex ($P<0.05$) myocytes (Figure 5, panels C and F). In adult mouse LV apex and free wall myocytes, which lack $I_{to,s}$ [19], the decay phases of the Kv currents are best described by the sum of 2 exponentials, reflecting $I_{to,f}$ and $I_{K,slow}$, and the noninactivating current, I_{ss} [19,20]. Mean ± SEM $I_{to,f}$ ($P<0.05$) and I_{Kslow} ($P<0.01$) densities were significantly lower in αMHC$^{403/+}$, than in WT, LV free wall myocytes (Figure 5C), whereas mean ± SEM I_{ss} and I_{K1} densities in αMHC$^{403/+}$ and WT LV free wall myocytes were not significantly different (Figure 5C; Table 2). Analysis of the Kv currents recorded from αMHC and WT LV apex myocytes (Figure 5, Panels D and E) also revealed small, but statistically significant ($P<0.05$), differences in $I_{K,peak}$ and $I_{K,slow}$ amplitudes/densities in LV apex cells from young male αMHC$^{403/+}$, compared with WT, mice (Figure 5F; Table 2). The densities of the other K^+ currents, $I_{to,f}$, I_{ss} and I_{K1}, in contrast, were similar in αMHC$^{403/+}$ and WT LV apex cells (Figure 5F; Table 2).

3.4. Transcriptional remodeling in αMHC$^{403/+}$ ventricles

It has been reported previously that ventricular hypertrophy is associated with the increased expression of several genes, including atrial natriuretic factor (*Anf*) and β-myosin heavy chain (*Myh7*), both of which are often considered as markers of cardiac hypertrophy [21,22]. Additional experiments were conducted, therefore, to quantify the expression levels of the transcripts encoding these proteins in ventricular tissues from young (10–12 week) male αMHC$^{403/+}$ mice prior to any evidence of LV myocyte or ventricular tissue hypertrophy. Quantitative RT-PCR analyses were performed using RNA prepared from tissues isolated from different regions (interventricular septum, LV free wall and LV apex) of the hearts of young (10–12 week old) male αMHC$^{403/+}$ and WT mice using previously described methods [16]. Using equal amounts of RNA, the expression levels of *Anf* and *Myh7*, as well as of control genes, were quantified [16]. As illustrated in Figure 6A, quantitative RT-PCR analyses revealed that expression of the transcript encoding *Anf* was significantly ($P<0.001$) higher in αMHC$^{403/+}$, compared with WT, septum, whereas *Myh7* expression levels in αMHC$^{403/+}$ and WT septum were indistinguishable (Figure 6A). Similar results were

obtained in analyses of RNA from WT and αMHC$^{403/+}$ LV free wall and LV apex, i.e., *Anf* expression was increased, whereas *Myh7* was not (Figure 6 B and C) (see Discussion).

Additional experiments were completed to determine the expression levels of the transcripts encoding the channel subunit proteins previously shown to encode the various functional voltage-gated K^+ channels ($I_{to,f}$, $I_{to,s}$, $I_{K,slow1}$, $I_{K,slow2}$) present in adult mouse ventricular myocytes [23–35]. These analyses revealed that the expression levels of several (but not all) K^+ channel subunits were lower in the αMHC$^{403/+}$, compared with WT, ventricular tissue samples (Figure 6). In the septum, for example, the transcripts encoding the $I_{K,slow2}$ channel pore forming (α) subunit *Kcnb1* (Kv2.1) [27], as well as *Kcnd3* (Kv4.3) [34] and the $I_{to,f}$ channel accessory subunit, *Kcnip2* (KChIP2) [29,31,35], were significantly lower in the αMHC$^{403/+}$, compared with the WT, samples, whereas the expression levels of other Kv channel subunits, including *Kcnd2* ($I_{to,f}$) [33] and *Kcna5* ($I_{K,slow1}$) [25,30,32], were similar in αMHC$^{403/+}$ and WT septum (Figure 6A). The expression levels of the transcripts encoding the I_{K1} channel subunits, *Kcnj2* (Kir2.1) and *Kcnj12* (Kir2.2) [36], and the two pore domain K^+ channel subunit *Kcnk3* (TASK-1), which has been suggested to contribute to I_{ss} in rat cardiomyocytes [37], were also lower in the αMHC$^{403/+}$, compared with WT, interventricular septum (Figure 6A) tissue samples (see Discussion).

Analyses of K^+ channel subunit expression levels in LV free wall and apex (Figure 6B and 6C) tissue samples from αMHC$^{403/+}$ and WT animals revealed similar differences. Specifically, *Kcnip2, Kcnb1, Kcnd3, Kcnk3, Kcnj2 and Kcnj12* expression levels were lower in LV free wall (Figure 6B) and LV apex (Figure 6C) from αMHC$^{403/+}$, compared with WT, animals. In addition, however, the transcript encoding the $I_{to,f}$ channel pore forming (α) subunit *Kcnd2* (Kv4.2) [33] was found to be expressed at lower levels in both LV wall (Figure 6B) and LV apex (Figure 6C) tissue samples from the αMHC$^{403/+}$ animals (see Discussion). In contrast, no significant differences in the expression levels of the transcripts encoding *Kcna4* (Kv1.4), *Kcna5* (Kv1.5) or *Kcnk2* (TREK-1) expression were detected in αMHC$^{403/+}$ and WT LV free wall and LV apex (see Discussion).

4. Discussion

4.1 Electrical remodeling precedes αMHC$^{403/+}$ ventricular myocyte hypertrophy

Consistent with previous studies [9,10], the experiments here revealed that LV hypertrophy is not detectable in 10–12 week old male αMHC$^{403/+}$ mice. Direct echocardiographic analyses and histological examination revealed no differences in LV wall thickness or in relative LV myocyte cross sectional area in 10–12 week old male αMHC$^{403/+}$ and WT animals. Although no structural LV hypertrophy was detected, electrocardiographic (ECG) abnormalities were observed in 10–12 week old male αMHC$^{403/+}$ mice. Analyses of surface ECG recordings obtained from pre-hypertrophic male αMHC$^{403/+}$ mice revealed that QT intervals were prolonged significantly ($P<0.001$), compared with age-matched WT animals.

Consistent with the lack of measureable ventricular hypertrophy in 10–12 week old male αMHC$^{403/+}$ mice, whole cell membrane capacitances measured in myocytes isolated from the interventricular septum and from the LV (apex and free wall) of αMHC$^{403/+}$ and WT animals were not significantly different (Table 2). Whole-cell voltage-clamp experiments,

however, revealed that peak outward K^+ current ($I_{K,peak}$) amplitudes/densities in myocytes isolated from the interventricular septum of 10–12 week old male αMHC$^{403/+}$ mice were significantly ($P<0.001$) lower than in septum cells isolated from WT mice. Analyses of the outward Kv current waveforms revealed that $I_{to,f}$ ($P<0.05$), $I_{to,s}$ ($P<0.001$) and $I_{K,slow}$ ($P<0.001$) amplitudes/densities in αMHC$^{403/+}$ interventricular septum myocytes were significantly lower than $I_{to,f}$, $I_{to,s}$ and $I_{K,slow}$ amplitudes/densities in septum cells from age matched littermate controls (Table 2). In marked contrast, I_{ss} and I_{K1} amplitudes/densities in αMHC$^{403/+}$ and WT interventricular septum myocytes were not significantly different (Table 2). Whole-cell voltage-clamp recordings also revealed attenuation of Kv currents in LV free wall and LV apex myocytes from αMHC$^{403/+}$, compared with WT, mice. Importantly, the reductions in the densities of the repolarizing K^+ currents reflect decreased K^+ current amplitudes only as no measureable differences in whole-cell membrane capacitances were observed. Interestingly, previous studies of electrical remodeling in pressure overload-induced pathological left ventricular hypertrophy [16] and in physiological hypertrophy [38] have also revealed that cellular hypertrophy and functional ion channel expression levels are differentially regulated. In addition, the observation that repolarizing K^+ current amplitudes are reduced in αMHC$^{403/+}$ LV cells suggests a mechanism for remodeling in response to the expression of the mutant αMHC$^{403/+}$ protein or alterations in downstream signaling pathways.

The experiments here also revealed regional differences in the effects of HCM on both the peak outward currents and the individual Kv current components. The magnitudes of the reductions in the amplitudes/densities of both $I_{K,peak}$ and $I_{K,slow}$, for example, were greater in interventricular septum myocytes than in either LV free wall or LV apex myocytes (Table 2). In addition, in αMHC$^{403/+}$ interventricular septum myocytes, mean ± SEM $I_{to,f}$ amplitude (density) was significantly lower than in WT septum cells, whereas mean ± SEM $I_{to,f}$ amplitudes/densities in αMHC$^{403/+}$ and WT LV free wall and LV apex myocytes were not significantly different (Table 2). Numerous previous studies have demonstrated that down-regulation of repolarizing K^+ currents and increased dispersion of ventricular repolarization in the context of pathological cardiac hypertrophy are potentially arrhythmogenic [39]. Interestingly, the marked regional differences in the remodeling of repolarizing Kv currents observed in the αMHC$^{403/+}$ mice would be expected to increase the dispersion of ventricular repolarization and be proarrhythmic.

4.2 Molecular remodeling in young αMHC$^{403/+}$ ventricles

Although the morphological and electrical measurements did not detect cellular or LV tissue hypertrophy in young αMHC$^{403/+}$ animals, quantitative RT-PCR analysis revealed that the expression of the hypertrophy marker, *Anf*, is increased several-fold in the interventricular septum in LV free wall and in the LV apex of young αMHC$^{403/+}$, compared with WT age-matched, mice, possibly suggesting an early molecular marker of pathology, i.e., prior to the measureable hypertrophy of LV ventricular myocytes in this model. Expression of the other hypertrophy marker, *Myh7*, however, was not increased in 10–12 week male αMHC$^{403/+}$ ventricles, consistent with the cellular and the functional data. It seems likely that increased *Anf* expression is an early marker of molecular remodeling that precedes hypertrophy in this

αMHC$^{403/+}$ model, as has been reported previously for other, molecularly similar, mouse models of hypertrophic cardiomyopathy [22].

The molecular analyses here also revealed rather small, but in some cases statistically significant, differences in the expression levels of several Kv channel subunits in αMHC$^{403/+}$ and WT ventricles, some of which appear to be correlated with changes in current amplitudes/densities. The electrophysiological experiments here, for example, revealed that $I_{K,slow}$ amplitudes/densities were decreased in αMHC$^{403/+}$ interventricular septum, LV free wall and LV apex myocytes (Table 2). The quantitative RT-PCR analysis, for example, revealed differences in the expression of *Kcnb1*, which underlies one component of $I_{K,slow}$, $I_{K,slow2}$ [27]. Significant differences were also observed in the expression levels of the *Kcnip2* transcript, which encodes the $I_{to,f}$ channel accessory subunit, KChIP2 [29,31,35], in αMHC$^{403/+}$ and WT interventricular septum, LV free wall, and LV apex. $I_{to,f}$ amplitudes/densities, however, were only different in (αMHC$^{403/+}$ and WT) interventricular myocytes, but not in LV free wall or LV apex myocytes. In addition, *Kcnd3* (Kv4.3), which does not contribute to the generation of mouse ventricular $I_{to,f}$ channels [34], is reduced in αMHC$^{403/+}$, compared with WT, interventricular septum, LV apex and LV free wall. In marked contrast, *Kcnd2*, which encodes the pore-forming subunit, Kv4.2, of mouse ventricular $I_{to,f}$ channels [33], is lower in the LV free wall and apex, but not the interventricular septum, of αMHC$^{403/+}$ hearts, whereas $I_{to,f}$ amplitudes/densities are lower in the αMHC$^{403/+}$, compared with WT, septum, but not in αMHC$^{403/+}$ LV free wall or apex myocytes. In addition, expression of the transcripts (*Kcnj2* and *Kcnj12*) encoding the inwardly rectifying K^+ (I_{K1}) channel subunits, Kir2.1 and Kir2.2, are significantly lower in αMHC$^{403/+}$, than in WT, interventricular septum, LV free wall and LV apex, whereas I_{K1} densities are not different. In contrast, no significant differences in *Kcna4*, which underlies $I_{to,s}$, expression in αMHC$^{403/+}$ and WT septum samples, were observed, although $I_{to,s}$ amplitudes/densities were significantly lower in αMHC$^{403/+}$, compared with WT, septum myocytes.

The observed differences in repolarizing K^+ current amplitudes/densities in αMHC$^{403/+}$ and WT LV myocytes, therefore, are not correlated with differences in the transcript expression levels of the underlying channel subunits, suggesting that post-transcriptional and/or post-translational mechanisms underlie the observed differences in K^+ current amplitudes/densities prior to the onset of cellular hypertrophy.

4.3 Conclusions

Despite increasing knowledge of the genetic underpinnings of familial HCM, the pathophysiological mechanisms linking identified genetic lesions to electrical dysfunction remain poorly understood. The pathogenesis of ventricular tachyarrhythmias, for example, the most common cause of sudden cardiac death in HCM, is not clear, although ventricular tachyarrhythmias have been suggested to be secondary to hypertrophy, myocardial ischemia, interstitial fibrosis, and abnormal Ca^{2+} homeostasis. The results presented here demonstrate that electrical remodeling in young (10–12 week old) male αMHC$^{403/+}$ mice is associated with electrocardiographic abnormalities, specifically QT interval prolongation, without evidence of LV hypertrophy or LV myocyte hypertrophy. The results of experiments

completed here also demonstrate marked reductions in the densities of repolarizing K^+ currents and that there are regional differences (e.g., in the interventricular septum, compared with the LV free wall and the LV apex) in K^+ current remodeling. Further studies focused on identifying the signaling pathways that trigger the electrical remodeling and result in QT prolongation in this model will be of considerable interest. Therapeutic strategies aimed at reducing the electrical remodeling of repolarizing K^+ channels would, therefore, appear to be a promising approach in the treatment of HCM-associated ventricular arrhythmias.

Acknowledgments

The authors thank Mr. Richard Wilson for maintaining and screening the mouse line ($\alpha MHC^{403/+}$) used in the studies described here. The financial support provided by the National Heart Lung and Blood Institute of the National Institutes of Health (HL084553 to JGS and CES; HL034161 and HL066388 to JMN), the Howard Hughes Medical Institute (CES) and the Department of Anesthesiology at Washington University Medical School is also gratefully acknowledged.

References Cited

1. Maron BJ, Shirani J, Poliac LC, Mathenge R, Roberts WC, Mueller FO. Sudden death in young competitive athletes. Clinical, demographic, and pathological profiles. JAMA. 1996; 276:199–204. [PubMed: 8667563]
2. Bonne G, Carrier L, Richard P, Hainque B, Schwartz K. Familial hypertrophic cardiomyopathy: from mutations to functional defects. Circ Res. 1998; 83:580–593. [PubMed: 9742053]
3. Frey N, Luedde M, Katus HA. Mechanisms of disease: hypertrophic cardiomyopathy. Nat Rev Cardiol. 2011; 9:91–100. [PubMed: 22027658]
4. Keren A, Syrris P, McKenna WJ. Hypertrophic cardiomyopathy: the genetic determinants of clinical disease expression. Nat Clin Pract Cardiovasc Med. 2008; 5:158–168. [PubMed: 18227814]
5. Maass A, Leinwand LA. Animal models of hypertrophic cardiomyopathy. Curr Opin Cardiol. 2000; 15:189–196. [PubMed: 10952427]
6. Geisterfer-Lowrance AA, Christe M, Conner DA, Ingwall JS, Schoen FJ, Seidman CE, et al. A mouse model of familial hypertrophic cardiomyopathy. Science. 1996; 272:731–734. [PubMed: 8614836]
7. Spindler M, Saupe KW, Christe ME, Sweeney HL, Seidman CE, Seidman JG, et al. Diastolic dysfunction and altered energetics in the alphaMHC$^{403/+}$ mouse model of familial hypertrophic cardiomyopathy. J Clin Invest. 1998; 101:1775–1783. [PubMed: 9541509]
8. Bevilacqua LM, Maguire CT, Seidman JG, Seidman CE, Berul CI. QT dispersion in alpha-myosin heavy-chain familial hypertrophic cardiomyopathy mice. Ped Res. 1999; 45:643–647.
9. Wolf CM, Moskowitz IP, Arno S, Branco DM, Semsarian C, Bernstein SA, et al. Somatic events modify hypertrophic cardiomyopathy pathology and link hypertrophy to arrhythmia. PNAS. 2005; 102:18123–18128. [PubMed: 16332958]
10. McConnell BK, Fatkin D, Semsarian C, Jones KA, Georgakopoulos D, Maguire CT, et al. Comparison of two murine models of familial hypertrophic cardiomyopathy. Circ Res. 2001; 88:383–389. [PubMed: 11230104]
11. Berul CI, Christe ME, Aronovitz MJ, Seidman CE, Seidman JG, Mendelsohn ME. Electrophysiological abnormalities and arrhythmias in alpha MHC mutant familial hypertrophic cardiomyopathy mice. J Clin Invest. 1997; 99:570–576. [PubMed: 9045856]
12. Uchiyama K, Hayashi K, Fujino N, Konno T, Sakamoto Y, Sakata K, et al. Impact of QT variables on clinical outcome of genotyped hypertrophic cardiomyopathy. Ann Noninvasive Electrocardiol. 2009; 14:65–71. [PubMed: 19149795]
13. Johnson JN, Grifoni C, Bos JM, Saber-Ayad M, Ommen SR, Nistri S, et al. Prevalence and clinical correlates of QT prolongation in patients with hypertrophic cardiomyopathy. Eur Heart J. 2011; 32:1114–1120. [PubMed: 21345853]

14. Jouven X, Hagege A, Charron P, Carrier L, Dubourg O, Langlard JM, et al. Relation between QT duration and maximal wall thickness in familial hypertrophic cardiomyopathy. Heart. 2002; 88:153–157. [PubMed: 12117842]
15. Christiaans I, Lekanne dit Deprez RH, van Langen IM, Wilde AA. Ventricular fibrillation in MYH7-related hypertrophic cardiomyopathy before onset of ventricular hypertrophy. Heart Rhythm. 2009; 6:1366–1369. [PubMed: 19539541]
16. Marionneau C, Brunet A, Flagg TP, Pilgram TK, Demolombe S, Nerbonne JM. Distinct cellular and molecular mechanisms underlie functional remodeling of repolarizing K^+ currents with left ventricular hypertrophy. Circ Res. 2008; 102:1406–1415. [PubMed: 18451341]
17. Speerschneider T, Thomsen MB. Physiology and analysis of the electrocardiographic T wave in mice. Acta Physiol. 2013; 209:262–271.
18. Roussel J, Champeroux P, Roy J, Richard S, Fauconnier J, Le Guennec JY. The complex QT/RR relationship in mice. Sci Rep. 2016; 6:25388. [PubMed: 27138175]
19. Xu H, Guo W, Nerbonne JM. Four kinetically distinct depolarization-activated K^+ currents in adult mouse ventricular myocytes. J Gen Physiol. 1999; 113:661–678. [PubMed: 10228181]
20. Brunet S, Aimond F, Li H, Guo W, Eldstrom J, Fedida D, et al. Heterogeneous expression of repolarizing, voltage-gated K^+ currents in adult mouse ventricles. J Physiol. 2004; 559:103–120. [PubMed: 15194740]
21. Mercadier JJ, Lompré AM, Wisnewsky C, Samuel JL, Bercovici J, Swynghedauw B, et al. Myosin isoenzyme changes in several models of rat cardiac hypertrophy. Circ Res. 1981; 49:525–532. [PubMed: 6454511]
22. Vikstrom KL, Bohlmeyer T, Factor SM, Leinwand LA. Hypertrophy, pathology, and molecular markers of cardiac pathogenesis. Circ Res. 1998; 82:773–778. [PubMed: 9562436]
23. Barry DM, Xu H, Schuessler RB, Nerbonne JN. Functional knockout of the transient outward current, long-QT synrome, and cardiac remodeling in mice expressing a dominant-negative Kv4 alpha subunit. Circ Res. 1998; 83:560–567. [PubMed: 9734479]
24. Zhou J, Jeron A, London B, Han X, Koren G. Characterization of a slowly inactivating outward current in adult mouse ventricular myocytes. Circ Res. 1998; 83:806–814. [PubMed: 9776727]
25. London B, Jeron A, Zhou J, Buckett P, Han X, Mitchell GF, et al. Long QT and ventricular arrhythmias in transgenic mice expressing the N terminus and first transmembrane segment of a voltage-gated potassium channel. PNAS. 1998; 95:2926–2931. [PubMed: 9501192]
26. Guo W, Xu H, London B, Nerbonne JM. Molecular basis of transient outward K^+ current diversity in mouse ventricular myocytes. J Physiol. 1999; 521:587–599. [PubMed: 10601491]
27. Xu H, Barry DM, Li H, Brunet S, Guo W, Nerbonne JM. Attenuation of the slow component of delayed rectification, action potential prolongation, and triggered activity in mice expressing a dominant-negative Kv2 alpha subunit. Circ Res. 1999; 85:623–633. [PubMed: 10506487]
28. Guo W, Li H, London B, Nerbonne JM. Functional consequences of elimination of $I_{to,f}$ and $I_{to,s}$): early afterdepolarizations, atrioventricular block, and ventricular arrhythmias in mice lacking Kv1. 4 and expressing a dominant-negative Kv4 alpha subunit. Circ Res. 2000; 87:73–79. [PubMed: 10884375]
29. Kuo HC, Cheng CF, Clark RB, Lin JJ, Lin JL, Hoshijima M, et al. A defect in the Kv channel-interacting protein 2 (KChIP2) gene leads to a complete loss of I_{to} and confers susceptibility to ventricular tachycardia. Cell. 2001; 107:801–813. [PubMed: 11747815]
30. London B, Guo W, Pan XH, Lee JS, Shusterman V, Rocco CJ, et al. Targeted replacement of Kv1. 5 in the mouse leads to loss of the 4-aminopyridine-sensitive component of $I_{K,slow}$ and resistance to drug-induced qt prolongation. Circ Res. 2001; 88:940–946. [PubMed: 11349004]
31. Guo W, Li H, Aimond F, Johns DC, Rhodes KJ, Trimmer JS, et al. Role of heteromultimers in the generation of myocardial transient outward K^+ currents. Circ Res. 2002; 90:586–593. [PubMed: 11909823]
32. Li H, Guo W, Yamada KA, Nerbonne JM. Selective elimination of $I_{K,slow1}$ in mouse ventricular myocytes expressing a dominant negative Kv1. 5alpha subunit. Am J Physiol Heart Circ Physiol. 2004; 286:H319–H328. [PubMed: 14527939]

33. Guo W, Jung WE, Marionneau C, Aimond F, Xu H, Yamada KA, et al. Targeted deletion of Kv4. 2 eliminates $I_{to,f}$ and results in electrical and molecular remodeling, with no evidence of ventricular hypertrophy or myocardial dysfunction. Circ Res. 2005; 97:1342–1350. [PubMed: 16293790]

34. Niwa N, Wang W, Sha Q, Marionneau C, Nerbonne JM. Kv4. 3 is not required for the generation of functional $I_{to,f}$ channels in adult mouse ventricles. J Mol Cell Cardiol. 2008; 44:95–104. [PubMed: 18045613]

35. Foeger NC, Wang W, Mellor RL, Nerbonne JM. Stabilization of Kv4 protein by the accessory K^+ channel interacting protein 2 (KChIP2) subunit is required for the generation of native myocardial fast transient outward K^+ currents. J Physiol. 2013; 591:4149–4166. [PubMed: 23713033]

36. Zaritsky JJ, Redell JB, Tempel BL, Schwarz TL. The consequences of disrupting cardiac inwardly rectifying K^+ current (I_{K1}) as revealed by the targeted deletion of the murine Kir2.1 and Kir2. 2 genes. J Physiol. 2001; 533:697–710. [PubMed: 11410627]

37. Putzke C, Wemhöner K, Sachse FB, Rinné S, Schlichthörl G, Li XT, et al. The acid-sensitive potassium channel TASK-1 in rat cardiac muscle. Cardiovasc Res. 2007; 75:59–68. [PubMed: 17389142]

38. Yang K-C, Tseng Y-T, Nerbonne JM. Exercise training and P13Kα-induced electrical remodeling is independent of cellular hypertrophy and Akt signaling. J Mol Cell Cardiol. 2012; 53:532–541. [PubMed: 22824041]

39. Nattel S, Maguy A, Le Bouter S, Yeh YH. Arrhythmogenic ion-channel remodeling in the heart: heart failure, myocardial infarction, and atrial fibrillation. Physiol Rev. 2007; 87:425–456. [PubMed: 17429037]

Highlights

- Cardiac hypertrophy is not evident on echocardiographic examination of young (10–12 week) αMHC$^{403/+}$ male mice.
- QT prolongation is marked in young (10–12 week) αMHC$^{403/+}$ male mice.
- Morphological and membrane capacitance measurements do not reveal hypertrophy of 10–12 week old male αMHC$^{403/+}$ ventricular myocytes.
- Repolarizing voltage-gated K^+ (Kv) current amplitudes/densities are reduced in ventricular myocytes isolated from young (10–12 week old) αMHC$^{403/+}$, compared with WT, mice.
- Transcriptional remodeling of K^+ channel subunits is evident in the ventricles of male (10–12 week old) αMHC$^{403/+}$ mice.

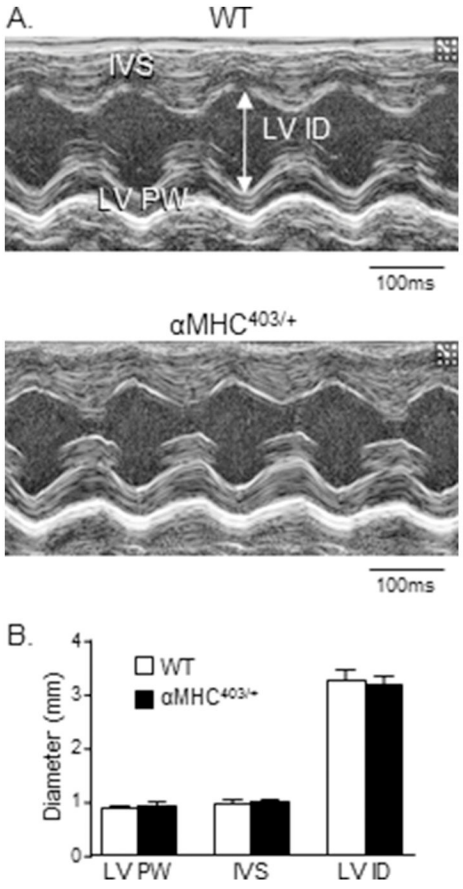

Figure 1. Transthoracic echocardiographic images reveal no significant abnormalities in diastolic LV wall dimensions in young (10–12 week) male αMHC$^{403/+}$ animals

(**A**) Representative transthoracic echocardiographic images (M-mode) of the interventricular septum and the LV posterior wall of 10–12 week old WT and αMHC$^{403/+}$ male mice. ***(B)*** No significant differences are evident in mean ± SEM diastolic LV posterior wall (LVPW) or interventricular septum (IVS) or left ventricular inner diameter (LVID) dimensions in WT (N = 8) and αMHC$^{403/+}$ (N = 8) mice.

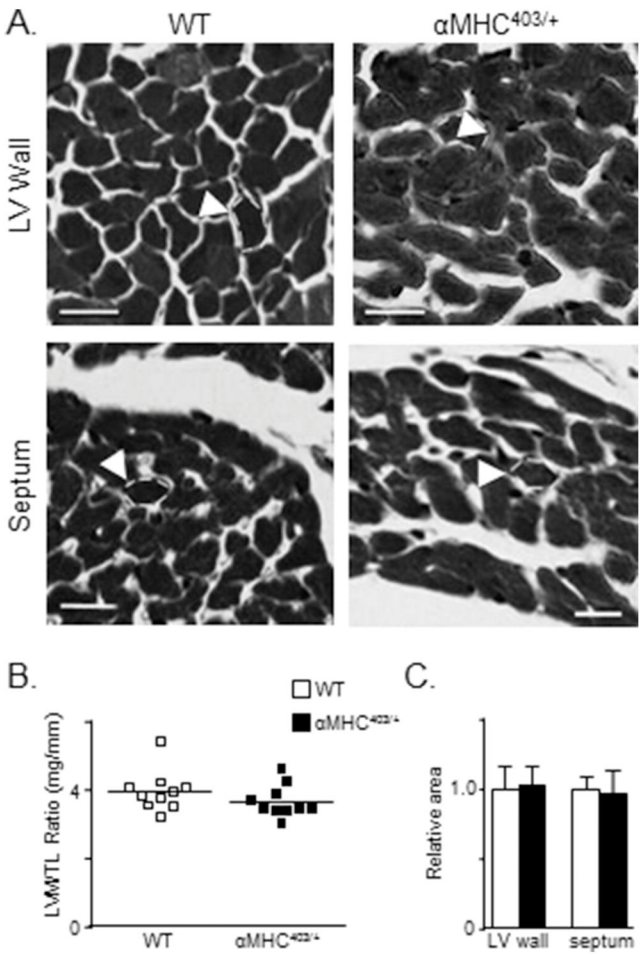

Figure 2. Cross-sectional areas of LV wall and septum myocytes in young (10–12 week) male WT and αMHC$^{403/+}$ mice are indistinguishable

(**A**) Representative transverse sections of the LV wall and interventricular septum in WT and αMHC$^{403/+}$ hearts, stained with Masson Trichrome, are shown. The white dashed lines were added to the images to outline the borders of individual myocytes (scale bar = 50 μm). ***(B)*** *LV mass/tibia length (LVM/TL) ratios, determined in WT (N = 10) and αMHC$^{403/+}$ (N = 10) animals (individual and mean values are shown), are not significantly different. (**C**) Mean ± SEM relative cross-sectional areas of both LV wall (n = 70) and interventricular septum myocytes (n = 65), measured in WT (N = 2) and αMHC$^{403/+}$ (N = 2) animals, are indistinguishable.*

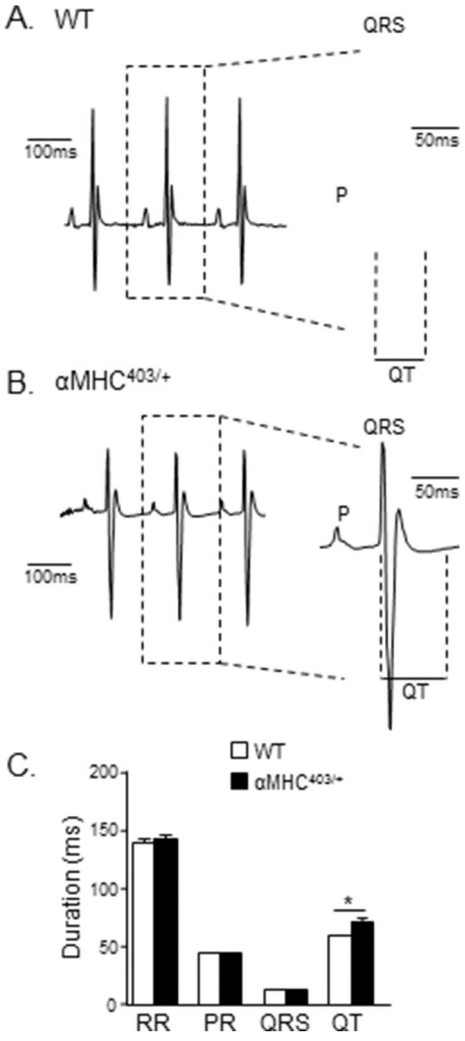

Figure 3. QT prolongation is evident in young (10–12 week) male αMHC$^{403/+}$ mice

Representative (lead II) ECG waveforms from anesthetized (**A**) WT and (**B**) αMHC$^{403/+}$ mice are shown; individual PQRST waveforms are shown on an expanded time scale on the right of each record. (**C**) Mean ± SEM RR, PR, and QRS intervals are indistinguishable in WT (N = 18) and αMHC$^{403/+}$ (N = 15) mice, whereas the mean ± SEM QT interval is significantly *(*P<0.001)* prolonged in αMHC$^{403/+}$ (N = 15), compared with WT (N = 18), mice.

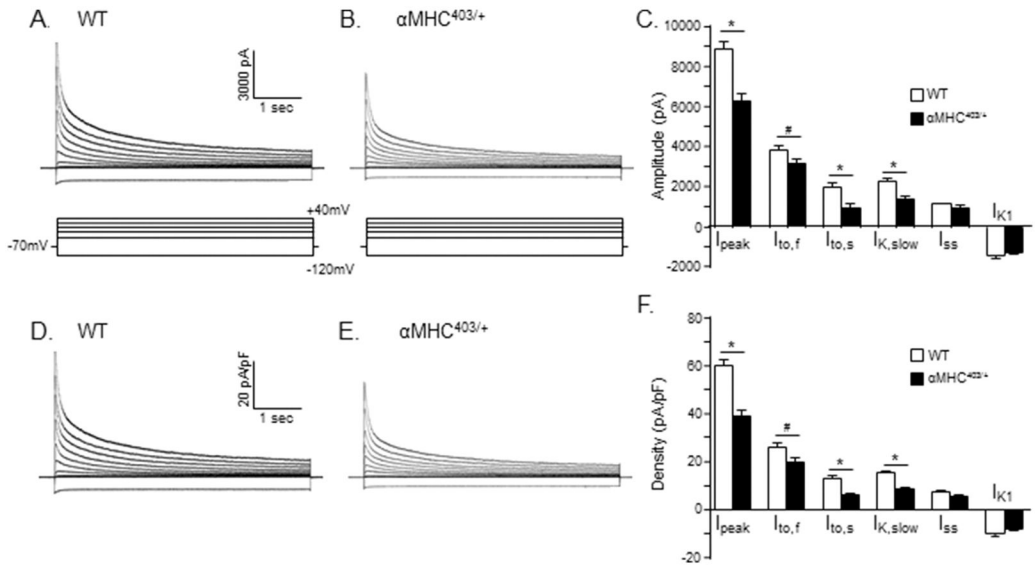

Figure 4. Repolarizing K^+ current amplitudes/densities are significantly lower in myocytes isolated from the interventricular septum of young (10–12 week) male αMHC$^{403/+}$, compared with WT, mice

Representative whole-cell K^+ current waveforms, recorded from isolated WT (**A**) and αMHC$^{403/+}$ (**B**) interventricular septum myocytes in response to (4.5 s) voltage steps to test potentials between −120 and +40 mV from a holding potential (HP) of −70 mV, as described in **Methods**, are shown; the protocol is illustrated below the current records. Peak outward K^+ currents were measured in each cell as the maximal outward current at +40 mV, and I_{K1} amplitudes in each cell were measured as the maximal inward current measured at −120 mV. The amplitudes of the individual Kv current components, $I_{to,f}$, $I_{to,s}$, $I_{K,slow}$ and I_{ss}, were determined from exponential fits to the decay phases of the total outward currents evoked at +40 mV. (**C**) Mean ± SEM $I_{K,peak}$, $I_{to,f}$, $I_{to,s}$, $I_{K,slow}$, I_{ss} and I_{K1} amplitudes in WT (n = 19; N = 4) and αMHC$^{403/+}$ (n = 11; N = 3) interventricular septum myocytes are plotted. The amplitudes of each of the currents in each cell were normalized to the whole-cell membrane capacitance (measured in the same cell) to provide current densities. Normalized current densities for the representative WT and αMHC$^{403/+}$ interventricular myocyte currents shown in (**A**) and (**B**) are presented in (**D**) and (**E**), respectively. Mean ± SEM $I_{K,peak}$, $I_{to,f}$, $I_{to,s}$, $I_{K,slow}$, I_{ss} and I_{K1} densities in WT (n = 19; N = 4) and αMHC$^{403/+}$ (n = 11; N = 3) myocytes are presented in (**F**). $^{*,\#}$ Values in WT and αMHC$^{403/+}$ are significantly different in αMHC$^{403/+}$, compared with WT, interventricular septum cells at the $^{*}P<0.001$ and $^{\#}P<0.05$ levels.

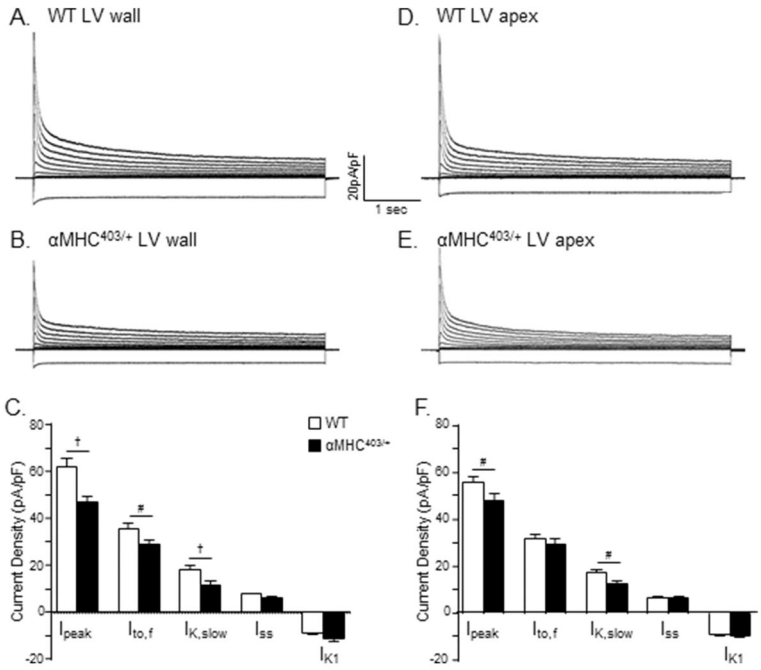

Figure 5. Peak outward K^+ current densities are also significantly lower in myocytes isolated from the LV free wall and from the LV apex of young (10–12 week) male αMHC$^{403/+}$, compared with WT, mice

Representative whole cell outward K^+ current waveforms, recorded from isolated WT (**A**) and αMHC$^{403/+}$ (**B**) LV wall myocytes, as described in the legend to Figure 4, are shown. Note that the currents were normalized to the whole-cell capacitance (in the same cell) and current densities are plotted. (**C**) Mean ± SEM $I_{K,peak}$, $I_{to,f}$ and $I_{K,slow}$ densities are significantly lower in αMHC$^{403/+}$ (n = 16; N = 4) than in WT (n = 13; N = 2), LV wall cells. Representative whole-cell K^+ current waveforms in WT (**D**) and αMHC$^{403/+}$ (**E**) LVapex myocytes, recorded as described in Figure 4, are also shown. (**F**) Mean ± SEM $I_{K,peak}$ and $I_{K,slow}$ densities are significantly lower in αMHC$^{403/+}$ (n = 11; N = 3), compared with WT (n = 21; N = 4), LV apex cells. $^{\dagger,\#}$Values in WT and αMHC$^{403/+}$ are significantly different at the $^{\dagger}P<0.01$ and $^{\#}P<0.05$ levels.

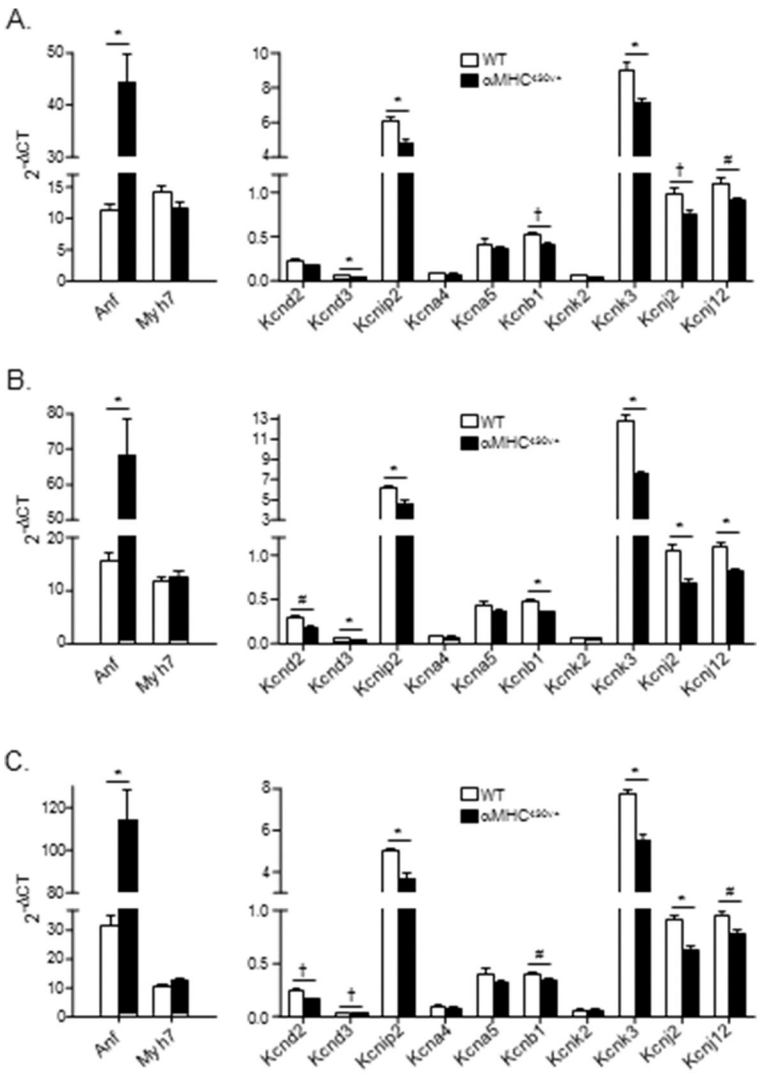

Figure 6. Expression levels of transcripts encoding several K^+ channel subunits are lower in LV isolated from young (10–12 week) male $\alpha MHC^{403/+}$, compared with WT, animals

Mean ± SEM RNA expression levels (arbitrary units) of hypertrophy markers and K^+ channel pore-forming and accessory subunits and WT (N = 6) and $\alpha MHC^{403/+}$ (N = 6) interventricular septum (**A**), LV wall (**B**) and LV apex (**C**) are shown. Indicated values are significantly *(*P<0.001; $^{\dagger}P$<0.01; $^{\#}P$<0.05) different in $\alpha MHC^{403/+}$ and WT samples.

Table 1

Sequence Specific Primers used in SYBR Green RT-PCR

Gene	Protein	Forward Primer	Reverse Primer
Anf	ANF	5'-CACTGTGGCGTGGTGAACA	5'-TCGTGATAGATGAAGGCAGGAA
Myh7	αMHC	5'-TGAATGAGCACCGGAGCAA	5'-CTGGCTGGTGAGGTCATTGA
Kcnd2	Kv4.2	5'-GCCGCAGCACCTAGTCGTT	5'-CACCACGTCGATGATACTCATGA
Kcnd3	Kv4.3	5'-CCTAGCTCCAGCGGACAAGA	5'-CCACTTACGTTGAGGACGATCA
Kcnip2	KChIP2	5'-GGCTGTATCACGAAGGAGGAA	5'-CCGTCCTTGTTTCTGTCCATC
Kcna4	Kv1.4	5'-AGAGGCGGATGAACCCACTA	5'-GCCCACCAAAACGCATCT
Kcna5	Kv1.5	5'-AAAGTGTCACCTAAAGGCCAAGAG	5'-CCAGACAGAGGGCATACAGAGA
Kcnb1	Kv2.1	5'-CACACAGCAATAGCGTTCAACTT	5'-AGGCGTAGACACAGTTCGGC
Kcnk2	TREK1	5'-CCTTTTGTGCCCAGACTGTTTC	5'-GCAAAGCATTCAGATTCATTCATAG
Kcnk3	TASK1	5'-GCTTCCGCAACGTCTATGC	5'-GGGATGGAGTACTGCAGCTTCT
Kcnj2	Kir2.1	5'-AAGAGCCACCTTGTGGAAGCT	5'-CCTTCTGAAGTGATCCTAGATTTGAGA
Kcnj12	Kir2.2	5'-AGCACCACCCTGACCACAAT	5' CTGAGCAACCCTACCCCAA
Hprt	HPRT	5'-TGAATCACGTTTGTGTCATTAGTGA	5'-TTCAACTTGCGCTCATCTTAGG

J Mol Cell Cardiol. Author manuscript; available in PMC 2018 February 01.

Table 2

Alterations in Repolarizing K^+ Currents in $\alpha MHC^{403/+}$ Ventricular Myocytes[1]

Cells	C_m (pF)		$I_{K,peak}$[2]	$I_{to,f}$[3]	$I_{to,s}$[3]	$I_{K,slow}$[3]	I_{ss}[3]	I_{K1}[2]
Septum								
WT	148 ± 5	Amplitude (pA)	8905 ± 376	3821 ± 239	1965 ± 202	2266 ± 174	1118 ± 77	−1470 ± 122
n=19		Density (pA/pF)	60.2 ± 2.2	26.2 ± 1.8	13.1 ± 1.1	15.2 ± 0.9	7.5 ± 0.3	−10.0 ± 0.7
		τ_{decay} (ms)		52 ± 1	413 ± 20	1922 ± 94		
$\alpha MHC^{403/+}$	160 ± 7	Amplitude (pA)	6264 ± 404*	3160 ± 211#	970 ± 158*	1414 ± 102*	943 ± 99	−1282 ± 107
n=11		Density (pA/pF)	39.3 ± 2.3*	20.1 ± 1.6#	5.9 ± 0.9*	8.8 ± 0.6*	6.1 ± 0.5	−8.2 ± 0.5
		τ_{decay} (ms)		51 ± 2	367 ± 28	2206 ± 234		
LV Wall								
WT	137 ± 8	Amplitude (pA)	8589 ± 682	4922 ± 511		2504 ± 240	1068 ± 71	−1209 ± 150
n=13		Density (pA/pF)	62.2 ± 3.7	35.5 ± 2.9		18.3 ± 1.7	7.8 ± 0.4	−8.6 ± 0.8
		τ_{decay} (ms)		63 ± 3		1100 ± 46		
$\alpha MHC^{403/+}$	126 ± 7	Amplitude (pA)	5898 ± 471†	3614 ± 359#		1513 ± 189†	798 ± 49	−1396 ± 139
n=16		Density (pA/pF)	46.9 ± 2.6†	28.8 ± 1.9#		11.9 ± 1.2†	6.5 ± 0.4	−10.4 ± 1.0
		τ_{decay} (ms)		56 ± 2		1245 ± 70		
LV Apex								
WT	147 ± 6	Amplitude (pA)	8276 ± 602	4675 ± 316		2601 ± 300	959 ± 64	−1309 ± 76
n=21		Density (pA/pF)	55.7 ± 2.2	31.8 ± 1.6		17.1 ± 1.2	6.5 ± 0.3	−9.0 ± 0.5
		τ_{decay} (ms)		70 ± 3		1217 ± 45		
$\alpha MHC^{403/+}$	151 ± 6	Amplitude (pA)	7201 ± 409#	4329 ± 364		1867 ± 139#	1005 ± 45	−1452 ± 93
n=11		Density (pA/pF)	48.1 ± 2.8#	29.0 ± 2.6		12.4 ± 0.9#	6.7 ± 0.4	−10.0 ± 0.6
		τ_{decay} (ms)		64 ± 2		1093 ± 42		

[1] All values are means ± SEM.

[2] Peak outward K^+ currents ($I_{K,peak}$), evoked at +40 mV from a holding potential (HP) of −70 mV, and inwardly rectifying K^+ currents, evoked at −120 mV from the same HP, were measured and normalized to the whole cell membrane capacitance (C_m) to provide current densities.

[3] The decay phases of the outward K^+ currents were fitted to the sum of three (septum) or two (LV wall and LV apex) exponentials to provide the amplitudes of the inactivating current components, $I_{to,f}$, $I_{to,s}$ and $I_{K,slow}$, the inactivation time constants (τ_{decay}) of $I_{to,f}$, $I_{to,s}$ and $I_{K,slow}$, and the amplitudes of I_{ss}. Currents in each WT and $\alpha MHC^{403/+}$ cell type (septum, LV wall and LV apex) were compared.

Values indicated are significantly (* $P \leq 0.001$, † $P \leq 0.01$, # $P \leq 0.05$) lower in $\alpha MHC^{403/+}$ cells than in WT cells.